

Dynamic atomic reconstruction: how Fe₃O₄ thin films evade polar catastrophe for epitaxy

Authors:

C. F. Chang,¹ Z. Hu,¹ S. Klein,^{2,†} X. H. Liu,¹ R. Sutarto,^{2,†} A. Tanaka,³ J. C. Cezar,^{4,†}
N. B. Brookes,⁴ H.-J. Lin,⁵ H. H. Hsieh,⁶ C. T. Chen,⁵ A. D. Rata,^{1,†} and L. H. Tjeng¹

Affiliations:

¹Max Planck Institute for Chemical Physics of Solids, Nöthnitzerstr. 40, 01187 Dresden, Germany

²II. Physikalisches Institut, Universität zu Köln, Zùlpicher Str. 77, 50937 Köln, Germany

³Department of Quantum Matter, ADSM, Hiroshima University, Higashi-Hiroshima 739-8530, Japan

⁴European Synchrotron Radiation Facility, 71 Avenue des Martyrs, Grenoble, France

⁵National Synchrotron Radiation Research Center, 101 Hsin-Ann Road, Hsinchu 30077, Taiwan

⁶Chung Cheng Institute of Technology, National Defense University, Taoyuan 335, Taiwan

[†] Current address;

S. Klein: Institute of Materials Physics in Space, German Aerospace Center, Linder Hohe, 51147 Köln, Germany;

R. Sutarto: Canadian Light Source, Saskatoon, Saskatchewan S7N 2V3, Canada;

J. C. Cezar: Laboratório Nacional de Luz Síncrotron, C.P. 6192, 13083-970 Campinas, SP, Brazil;

A. D. Rata: Institute for Physics, Martin-Luther-University, Halle-Wittenberg, 06099 Halle, Germany;

Abstract:

Polar catastrophe at the interface of oxide materials with strongly correlated electrons has triggered a flurry of new research activities. The expectations are that the design of such advanced interfaces will become a powerful route to engineer devices with novel functionalities. Here we investigate the initial stages of growth and the electronic structure of the spintronic $\text{Fe}_3\text{O}_4/\text{MgO}$ (001) interface. Using soft x-ray absorption spectroscopy we have discovered that the so-called A-sites are completely missing in the first Fe_3O_4 monolayer. This allows us to develop an unexpected but elegant growth principle in which during deposition the Fe atoms are constantly on the move to solve the divergent electrostatic potential problem, thereby ensuring epitaxy and stoichiometry at the same time. This growth principle provides a new perspective for the design of interfaces.

Subject areas: Condensed Matter Physics, Magnetism, Strongly Correlated Materials, Materials Science, Spintronics, Chemical Physics, Nanophysics

Main Text:

Physical properties of surfaces and interfaces of solids could markedly differ from those in the bulk, especially in cases when the surface or interface involves non-neutral crystal planes. For insulators, these polar planes cause the electrostatic potential to diverge, and thus to destabilize the system dramatically. The surface or interface is then forced to reconstruct, for example, by forming facets or defects. Or more spectacular, it could give up a substantial amount of charge, thereby altering its electronic structure completely [1–3]. Recently, claims have been made that such happens at the $\text{SrTiO}_3/\text{LaAlO}_3$ interface since the interface is conducting while the two constituents separately are good insulators [4, 5]. In fact, the formation of a two-dimensional electron gas and the occurrence of superconductivity in this interface has generated frantic efforts worldwide to explore the potential of these interfaces for device applications [6–12] as well as to search for new emergent phenomena such as quantum criticality in 2-dimensional electron gas systems [13–15]. However, the growth process of these interfaces and polar interfaces in general is a mystery. How do the atoms rearrange themselves during the deposition or growth such that a well ordered and smooth interface is formed, despite the destabilizing forces due to the catastrophic electrostatic potential? Understanding the growth principles will widen the scope of interfaces that

one may want to design: interfaces which appear impossible to grow at first sight may now be tried out.

Here, we investigate the polar interface between Fe_3O_4 and the MgO (001) substrate, one of the most used interfaces in the research field of spintronics. [16-24] This interface is completely not understood in terms of atomic structure, electronic structure and growth mode. Figs. 1 (a), and (b) illustrate how the Fe_3O_4 inverse spinel crystal structure consisting of Fe^{3+} ions in tetrahedral coordination (A-sites), Fe^{2+} and Fe^{3+} ions (or on average $\text{Fe}^{2.5+}$) in octahedral coordination (B-sites) with O^{2-} ions in an fcc-lattice builds up the polar catastrophe problem. We have prepared the system using molecular beam epitaxy (MBE). This deposition method allows for a layer-by-layer growth of the Fe_3O_4 under ultra high vacuum conditions which facilitates the use of *in-situ* characterization techniques with surface monolayer sensitivity. The MBE growth of Fe_3O_4 on MgO (001) is also known to produce films with excellent physical properties [22]. In order to obtain direct insight into the atomic and electronic structure of the interface, we utilize soft x-ray absorption spectroscopy (XAS) at the Fe $L_{2,3}$ edges. This spectroscopic technique is extremely sensitive to the local coordination and charge state of the Fe ions [25–28].

Fe_3O_4 thin films with thicknesses varying between 0.67 and 8 monolayers (ML) were grown on MgO (001). Each film has been grown on a new and freshly annealed substrate. The substrate temperature was kept at 250 °C during the growth in order to avoid the Mg inter-diffusion at the $\text{Fe}_3\text{O}_4/\text{MgO}$ interface [29,30]. Details about the film growth are given in the Supplementary Materials [31]. One ML consists of one (001)-oriented layer of oxygen anions together with the appropriate number of Fe cations to maintain charge neutrality and stoichiometry, and has a thickness of 2.1 Å. In Fig. 1 (c), and (d) we present representative reflection high energy electron diffraction (RHEED) and low energy electron diffraction (LEED) patterns, respectively, of a 200 nm thick Fe_3O_4 film to demonstrate that the surface is still smooth for very long deposition times. The typical $(\sqrt{2} \times \sqrt{2})\text{R}45^\circ$ surface reconstruction is also clearly visible. Fig. 1 (e) shows the regular oscillations with time in the intensity of the specularly reflected RHEED beam during growth, indicating a two-dimensional layer-by-layer growth mode. Fig. 1 (f) displays the resistivity as a function of temperature from a 10 nm and a 200 nm film, showing the presence of the characteristic Verwey transition [22].

Figure 2 depicts the room temperature Fe L_3 XAS spectra of Fe_3O_4 films with thicknesses varying from 0.67 ML to 8 ML, and of a Fe_3O_4 bulk single crystal. A Fe_2O_3 single crystal was

measured simultaneously in a separate chamber to serve as energy reference for Fe L_3 edge. Further XAS experimental details and display of the entire Fe $L_{2,3}$ spectral range are given in the Supplementary Materials [31, Fig. S1]. We also include in Fig. 2 the spectra of bulk YBaCo₃FeO₇ [28], bulk FeO (reproduced from Ref. 32) and bulk Fe₂O₃ as references for Fe³⁺ ions in tetrahedral coordination, Fe²⁺ ions in octahedral coordination, and Fe³⁺ ions in octahedral coordination, respectively. The line shapes of the spectra strongly depend on the multiplet structure given by the atomic like Fe $3d-3d$ and $2p-3d$ Coulomb and exchange interactions, as well as by local crystal fields and the hybridization with the O $2p$ ligands [25–28]. Here we note the striking similarities of the spectral features of the 8 ML Fe₃O₄ thin film and the bulk magnetite, which confirms that our Fe₃O₄ films have the correct stoichiometry.

We now focus on the thickness dependence of the spectra. Clear and systematic changes can be observed, in particular in the peak position of the spectral feature labeled as (I) and in the intensity of the spectral feature labeled as (II) relative to that of peak (I), see Fig. 2. The position of peak (I) of the thinnest Fe₃O₄ films, *i.e.* of the 0.67, 0.75 and 1 ML films, is the same as that of bulk Fe₂O₃, while for the thicker films, *i.e.* 2 ML and beyond, it is more similar to that of bulk YBaCo₃FeO₇. This gives a first indication that the thinnest films contain only tiny amounts of Fe³⁺ ions in tetrahedral coordination and implies that such A-site Fe ions could essentially only be present for films of 2 ML thickness and beyond. This then would also explain why for the thinnest films one can see two separate peaks (I) and (II) like in bulk Fe₂O₃ (green curve), while for thicker films the appearance of an in-between peak associated with the Fe³⁺ ions in tetrahedral coordination (red curve) will fill up the valley between peak (I) and (II), making peak (II) to become a shoulder and the position of the larger peak (I) to shift to lower energies. Important is to note that the foot at the onset of the Fe L_3 edge, *i.e.* the feature between 706 and 707.7 eV, which is part of the spectral feature characteristic for Fe²⁺ ions in octahedral B sites (see blue curve), are thickness independent. All these strongly suggest that the spectral weight of the A-site and the B-site Fe³⁺ ions varies strongly with thickness.

To interpret and better understand the XAS spectra and their thickness dependence we have performed calculations using the well established configuration interaction cluster model that includes the full atomic multiplet theory and the local effects of the solid [25–28]. We have simulated each of the XAS spectra shown in Fig. 2 and obtained the spectral weight of the different Fe sites; computational details and fits are given in the Supplementary Materials [31,

Figs. S2, S3, and S4, 33]. The results are plotted as closed squares in the top panel of Fig. 3, where the error bars reflect the deviations of the fits to the experimental data. From the relative concentrations of the constituents we have calculated the average valence or equivalently, by taking the oxygen lattice to be complete, we have determined the Fe content y in our Fe_yO films. These y values are plotted as black closed squares in the bottom panel of Fig. 3. We can observe that all points are very close to the $\text{Fe}_{3/4}\text{O}$ (gray) line, which confirms the correct stoichiometry of our films through the entire thickness range and very consistent with the RHEED intensity oscillations which have a constant time period, *i.e.* independent of the film thickness.

An important aspect that emerges directly from the simulations is the strong thickness dependence of the different Fe constituents, see Fig. 3. We recall that bulk Fe_3O_4 has 1/3 (33%) Fe^{3+} ions in tetrahedral coordination (A-sites), 1/3 (33%) Fe^{2+} and 1/3 (33%) Fe^{3+} ions in octahedral coordination (B-sites). We found to our surprise that the amount of A-site Fe^{3+} ions is practically negligible for the thinnest films, *i.e.* 2-3% instead of the 33% bulk value. At the same time, the amount of B-site Fe^{3+} in the thinnest films is between 60-68%, much larger than the 33% bulk value. We also observe that with increasing film thickness the A-site Fe^{3+} amount increases and the B-site Fe^{3+} decreases, both to approach the 33% bulk value, see for example the 8 ML results in Fig. 3. Interestingly, the amount of B-site Fe^{2+} is rather constant and independent of the film thickness, it fluctuates around the 33% bulk value.

These spectroscopic findings provide crucial data for the determination of the actual growth process and the interface structure. Especially the observation that the first monolayer of the Fe_3O_4 film has essentially no A-sites is a surprising piece of information. In fact, as far as the monolayer is concerned, the choice of 'nature' not to have A-sites is the simplest manner to solve the planar electrostatic potential problem. As can be seen from Figs. 1 (a) and (b), it is indeed the presence of the A-sites that causes the polar catastrophe to occur as there are no negative ions in those A-site planes to neutralize the charges. So by not having A sites for the first monolayer, there is also no electrostatic problem. What we then have is that the first monolayer constitutes basically of a charge-neutral non-polar rocksalt FeO layer with 25% Fe vacancies. All Fe ions are occupying the B-site with 33% of them having the 2+ valence and 67% the 3+ state and the vacancies are not ordered since we did not observe any superstructure. We have also carried out polarization dependent XAS measurements, and we are able to indeed verify in detail that also the dichroic spectrum is consistent with the 33% Fe^{2+} and 67% Fe^{3+} B-site occupation. See Supplemental

Materials [31, Figs. S5]. Please note that these XAS spectra and the dichroism therein are very different from those of Fe atoms on MgO [34]. Moreover, capping this monolayer with a thick layer of MgO induces spectral weight changes that are fully consistent with the presence of 25% Fe vacancies. See Supplemental Materials [31, Fig. S6, 33].

For the second monolayer, we observe in the experiment the appearance of some amount of A-sites, about 16.7%, see top panel of Fig. 3. We now can arrive at the following model, see Fig. 4 where the left panel shows the growth process and the right panels the corresponding net charges, electric field, and electric potential of each plane. Since in bulk magnetite, a monolayer per unit cell includes 2 A-site Fe^{3+} , 2 B-site Fe^{2+} , 2 B-site Fe^{3+} , and 8 oxygen ions, we will use the formula notation Fe_6O_8 instead of $\text{Fe}_{3/4}\text{O}$ to describe each monolayer. When deposited, the second monolayer will first form a non-polar monolayer, like the first monolayer. Then, both the first and the second layers give away one Fe^{3+} ion as shown in Fig. 4 (b) to the space in between them to form a layer with two A-site Fe^{3+} ions. The entire film remains then also non-polar: a 6+ charge-layer is sandwiched by two 3- charge-layers. The electric field oscillates symmetrically around zero, and the electric potential remains nullified. In this model, there are two A-sites per 2 ML formula unit, *i.e.* the A-site concentration is $2/(2 \times 6) = 16\%$, which is very close to the experiment. The remaining outer Fe_5O_8 (defective rocksalt) layers contain each three Fe^{3+} and two Fe^{2+} B-site ions. The concentration of the Fe^{2+} B-site ions is thus $(2 \times 2)/(2 \times 6) = 33\%$, *i.e.* the same as for the first monolayer and consistent with the experiment, see top panel of Fig. 3.

For a 3-ML film, the layer added will again form a non-polar monolayer first. This monolayer and the subsurface monolayer then carry out the same process in which both give away one Fe^{3+} ion to the space in between. See Fig. 4 (c). Again, the potential divergence remains nullified after this process as shown on the most right panel of Fig. 4 (c). One complete bulk Fe_6O_8 layer now is formed. This growth process is repeated for the subsequent layers, and the model predicts that the concentration of the A-site ions will increase following the geometrical series $2(n-1)/6n$, while the concentration of the Fe^{2+} B-site ions will remain constant at $2n/6n = 33\%$ and that of the Fe^{3+} B-site ions will decrease following $2(n+1)/6n$, where n denotes the number of monolayers. These predictions of the model are also presented in Fig. 3. We can see that the essential behavior observed in the experiment is well reproduced with convergence to the bulk values for thicker films. We also would like to note that an ordering in the outer Fe_5O_8 layer can be made consistent with the often observed $(\sqrt{2} \times \sqrt{2})\text{R}45^\circ$ surface reconstruction in thicker (001) Fe_3O_4 films, please see the

Supplementary Materials for details [31].

We thus have found that the A-sites are absent in the first monolayer or interface, and that Fe ions are on the move while the film is growing to accommodate for the presence of A-sites inside the film having the proper crystal structure and stoichiometry. We clearly have a 'dynamic atomic reconstruction' taking place here.

It is interesting to note that the Fe_3O_4 thin films are insulating and that the interface does not induce metallicity as shown by the resistivity measurements displayed in Fig. 1 (f). This is obviously in contrast with the resistivity measurements on $\text{SrTiO}_3/\text{LaAlO}_3$ [5,35–37] and $\text{SrTiO}_3/\text{RETiO}_3$ [13–15]. In principle, the Fe_5O_8 interface layer could have been conducting since this layer can be considered as a defective and doped rocksalt FeO layer. Yet, considering the fact that small polaron effects in bulk Fe_3O_4 are strong and hamper the conductivity [38–40], we may expect that this will also be the case for the interface layer. Its resistivity will then be dominated by strong scattering effects due to disorder.

Our findings have direct and important implications for the field of Fe_3O_4 spintronics. There are some reports concerning the possible existence of a magnetically dead layer at the interface [41–43], but others ascribe the decrease of the magnetization in the thin films to the presence of antiphase boundaries leading to superparamagnetic behavior of the domains [44–46]. Our findings may give credit to the proponents of the dead magnetic layer model. In view of the absence or low amount of A-sites in the interface region, some of the superexchange paths which determine the ferrimagnetism in Fe_3O_4 are certainly missing. This then would also explain why tunneling experiments have spin-polarizations different than expected from the properties of bulk Fe_3O_4 [47]. We now can propose that the insertion of a monolayer of magnetic metals like Fe, Co, Ni, or even noble metals like Cu, Ag, Au or Pt between the Fe_3O_4 and the insulating oxide substrate will drastically change the situation: the metal layer inserted will act as a charge reservoir that can accommodate the flow of planar charges required to stabilize a Fe_3O_4 interface layer which has A-sites like in the bulk. The occurrence of a magnetically dead layer can then be prevented and also the spin polarization at the interface may be increased. A hint that the latter is not unrealistic can be found in an early work by Dedkov *et al.* [48] on oxidized Fe films deposited on metal substrates.

To summarize, using soft x-ray absorption spectroscopy we find that nature provides us with an unexpected but elegant solution for the polar catastrophe problem at the $\text{Fe}_3\text{O}_4/\text{MgO}$ (001)

interface: the A-site Fe^{3+} ions are missing in the first Fe_3O_4 layer and the growth process involves movements of not only the surface but also the subsurface Fe ions, securing epitaxy and stoichiometry at the same time. Having identified this ‘dynamic atomic reconstruction’ growth principle, we conclude that we really have to think differently and openly about how polar interfaces can grow. Apparently, ‘nature’ offers us a much wider range of opportunities to prepare unstable polar interfaces. It would be interesting to put effort to grow a monolayer or a few monolayer of Fe_3O_4 film where the defects are ordered, so that diffraction techniques can confirm the growth model.

Acknowledgments:

The research in Köln was supported by the Deutsche Forschungsgemeinschaft through SFB 608. The research of X. H. L. was supported by the Max Planck-POSTECH Center for Complex Phase Materials.

References:

1. A. Zangwill, *Physics at surfaces* (Cambridge University Press) (1988).
2. C. Noguera, *Physics and chemistry at oxide surfaces* (Cambridge University Press) (1996).
3. R. Hesper, L. H. Tjeng, A. Heres, and G. A. Sawatzky, *Photoemission evidence of electronic stabilization of polar surfaces in K_3C_{60}* , Phys. Rev. B **62**, 16046 (2000).
4. Satoshi Okamoto and Andrew J. Millis, *Electronic reconstruction at an interface between a Mott insulator and a band insulator*, Nature **428**, 630 (2004).
5. A. Ohtomo and H.Y. Hwang, *A high-mobility electron gas at the $\text{LaAlO}_3/\text{SrTiO}_3$ heterointerface*, Nature **427**, 423 (2004).
6. M. Huijben, A. Brinkman, G. Koster, G. Rijnders, H. Hilgenkamp, and D. H. A. Blank, *Structure-Property Relation of $\text{SrTiO}_3/\text{LaAlO}_3$ Interfaces*, Adv. Mat. **21**, 1665 (2009).
7. J. Mannhart and D.G. Schlom, *Oxide Interfaces—An Opportunity for Electronics*, Science **327**, 1607 (2010).
8. S.A. Chambers, M.H. Engelhard, V. Shutthanandan, Z. Zhu, T.C. Droubay, L. Qiao, P.V. Sushko,

- T. Feng, H.D. Lee, T. Gustafsson, E. Garfunkel, A.B. Shah, J.-M. Zuo, and Q.M. Ramasse, *Instability, intermixing and electronic structure at the epitaxial $\text{LaAlO}_3/\text{SrTiO}_3(001)$ heterojunction*, Surf. Sci. Rep. **65**, 317 (2010).
9. S.A. Chambers, *Understanding the mechanism of conductivity at the $\text{LaAlO}_3/\text{SrTiO}_3(001)$ interface*, Surf. Sci. **605**, 1133 (2011).
 10. H. Y. Hwang, Y. Iwasa, M. Kawasaki, B. Keimer, N. Nagaosa, and Y. Tokura, *Emergent phenomena at oxide interfaces*, Nat. Mat. **11**, 103 (2012).
 11. M. Salluzzo, S. Gariglio, X. Torrelles, Z. Ristic, R. Di Capua, J. Drnec, M. Moretti Sala, G. Ghiringhelli, R. Felici, and N. B. Brookes, *Structural and Electronic Reconstructions at the $\text{LaAlO}_3/\text{SrTiO}_3$ Interface*, Adv. Mater. **25**, 2333 (2013).
 12. A. Janotti, L. Bjaalie, L. Gordon, and C. G. Van de Walle, *Controlling the density of the two-dimensional electron gas at the $\text{SrTiO}_3/\text{LaAlO}_3$ interface*, Phys. Rev. B **86**, 241108 (2012).
 13. Pouya Moetakef, Daniel G. Ouellette, James R. Williams, S. James Allen, Leon Balents, David Goldhaber-Gordon, and Susanne Stemmer, *Quantum oscillations from a two-dimensional electron gas at a Mott/band insulator interface*, Appl. Phys. Lett. **101**, 151604 (2012).
 14. Clayton A. Jackson, Jack Y. Zhang, Christopher R. Freeze, and Susanne Stemmer, *Quantum critical behaviour in confined SrTiO_3 quantum wells embedded in antiferromagnetic SmTiO_3* , Nat. Commun. 5:4258 doi: 10.1038/ncomms5258 (2014).
 15. Santosh Raghavan, Jack Y. Zhang, and Susanne Stemmer, *Two-dimensional electron liquid at the (111) $\text{SmTiO}_3/\text{SrTiO}_3$ interface*, Appl. Phys. Lett. **106**, 132104 (2015).
 16. R. A. de Groot, F. M. Mueller, P. G. van Engen, and K. H. J. Buschow, *New Class of Materials: Half-Metallic Ferromagnets*, Phys. Rev. Lett. **50**, 2024 (1983).
 17. A. Yanase, and K. Siratori, *Band Structure in the High Temperature Phase of Fe_3O_4* , J. Phys. Soc. Japan **53**, 312 (1984).
 18. S.A. Chambers, *Epitaxial growth and properties of thin film oxides*, Surf. Sci. Reports **39**, 105 (2000).
 19. M Ziese, *Extrinsic magnetotransport phenomena in ferromagnetic oxides*, Rep. Prog. Phys. **65** 143 (2002).

20. R. Pentcheva, F. Wendler, H. L. Meyerheim, W. Moritz, N. Jedrecy, and M. Scheffler, *Jahn-Teller Stabilization of a Polar Metal Oxide Surface: $Fe_3O_4(001)$* , Phys. Rev. Lett. **94**, 126101 (2005).
21. Jean-Baptiste Moussy, *From epitaxial growth of ferrite thin films to spin-polarized tunneling*, J. Phys. D: Appl. Phys. **46** 143001 (2013).
22. X. H. Liu, A. D. Rata, C. F. Chang, A. C. Komarek, and L. H. Tjeng, *Verwey transition in Fe_3O_4 thin films: Influence of oxygen stoichiometry and substrate-induced microstructure*, Phys. Rev. B **90**, 125142 (2014).
23. R. Bliem, E. McDermott, P. Ferstl, M. Setvin, O. Gamba, J. Pavelec, M. A. Schneider, M. Schmid, U. Diebold, P. Blaha, L. Hammer, and G. S. Parkinson, *Subsurface cation vacancy stabilization of the magnetite(001) surface*, Science **346**, 1215 (2014).
24. Scott A. Chambers, *Stability at the surface*, Science **346** 1186 (2014).
25. F. M. F. de Groot, J. Electron Spectrosc. Relate. Phenom. **67**, 529 (1994).
26. A. Tanaka and T. Jo, Phys. Soc. Jpn. **63**, 2788 (1994).
27. T. Burnus, Z. Hu, Hua Wu, J. C. Cezar, S. Niitaka, H. Takagi, C. F. Chang, N. B. Brookes, H.-J. Lin, L. Y. Jang, A. Tanaka, K. S. Liang, C. T. Chen, and L. H. Tjeng, *X-ray absorption and x-ray magnetic dichroism study on Ca_3CoRhO_6 and Ca_3FeRhO_6* , Phys. Rev. B **770** 205111 (2008).
28. N. Hollmann, Z. Hu, M. Valldor, A. Maignan, A. Tanaka, H. H. Hsieh, H.-J. Lin, C. T. Chen, and L. H. Tjeng, *Electronic and magnetic properties of the kagome systems $YBaCo_4O_7$ and $YBaCo_3MO_7$ ($M=Al, Fe$)*, Phys. Rev. B **80**, 085111 (2009).
29. Y. J. Kim, Y. Gao, and S. A. Chambers, *Selective growth and characterization of pure, epitaxial $\alpha-Fe_2O_3$ (0001) and Fe_3O_4 (001) films by plasma-assisted molecular beam epitaxy*, Surface Science **371**, 358 (1997).
30. J. F. Anderson, Markus Kuhn, Ulrike Diebold, K. Shaw, P. Stoyanov, and D. Lind, *Surface structure and morphology of Mg-segregated epitaxial Fe_3O_4 (001) thin films on MgO (001)*, Phys. Rev. B. **56**, 9902 (1997).
31. See Supplemental Materials at [URL] for details of the thin film growth, the XAS experimental details and the entire Fe $L_{2,3}$ spectral range, the XAS spectra computational details, and the

$(\sqrt{2} \times \sqrt{2})R45^\circ$ surface reconstruction which is consistent with the Fe_5O_8 surface as proposed from our model.

32. J. H. Park, Ph.D. thesis, University of Michigan (1994).
33. T. Haupricht, R. Sutarto, M. W. Haverkort, H. Ott, A. Tanaka, H. H. Hsieh, H.-J. Lin, C. T. Chen, Z. Hu, and L. H. Tjeng, *Local electronic structure of Fe^{2+} impurities in MgO thin films: Temperature-dependent soft x-ray absorption spectroscopy study*, Phys. Rev. B **82**, 035120 (2010).
34. S. Baumann, F. Donati, S. Stepanow, S. Rusponi, W. Paul, S. Gangopadhyay, I. G. Rau, G. E. Pacchioni, L. Gragnaniello, M. Pivetta, J. Dreiser, C. Piamonteze, C. P. Lutz, R. M. Macfarlane, B. A. Jones, P. Gambardella, A. J. Heinrich, and H. Brune, *Origin of Perpendicular Magnetic Anisotropy and Large Orbital Moment in Fe Atoms on MgO*, Phys. Rev. Lett. **115**, 237202 (2015).
35. M. Huijben, G. Rijnders, D. H. A. Blank, S. Bals, S. V. Aert, J. Verbeeck, G. V. Tendeloo, A. Brinkman and H. Hilgenkamp, *Electronically coupled complementary interfaces between perovskite band insulators*, Nat. Mat. **5**, 556 (2006).
36. S. Thiel, G. Hammerl, A. Schmehl, C. W. Schneider, and J. Mannhart, *Tunable Quasi-Two-Dimensional Electron Gases in Oxide Heterostructures*, Science **313**, 1942 (2006).
37. M.P. Warusawithana, C. Richter, J.A. Mundy, P. Roy, J. Ludwig, S. Paetel, T. Heeg, A.A. Pawlicki, L.F. Kourkoutis, M. Zheng, M. Lee, B. Mulcahy, W. Zander, Y. Zhu, J. Schubert, J.N. Eckstein, D.A. Muller, C. Stephen Hellberg, J. Mannhart, and D.G. Schlom, *LaAlO_3 stoichiometry is key to electron liquid formation at $\text{LaAlO}_3/\text{SrTiO}_3$ interfaces*, Nat. Commun. **4**:2351 doi: 10.1038/ncomms3351 (2013).
38. J.-H. Park, L. H. Tjeng, J. W. Allen, P. Metcald, and C. T. Chen, *Single-particle gap above the Verwey transition in Fe_3O_4* , Phys. Rev. B **55**, 12813 (1997).
39. D. Schrupp, M. Sing, M. Tsunekawa, H. Fujiwara, S. Kasai, A. Sekiyama, S. Suga, T. Muro, V. A. M. Brabers, and R. Claessen, *High-energy photoemission on Fe_3O_4 : Small polaron physics and the Verwey transition*, Europhys. Lett. **70**, 789 (2005).
40. M. Kimura, H. Fujiwara, A. Sekiyama, J. Yamaguchi, K. Kishimoto, H. Sugiyama, G. Funabashi, S. Imada, S. Iguchi, Y. Tokura, A. Higashiya, M. Yabashi, K. Tamasaku, T. Ishikawa,

- T. Ito, S. Kimura, and S. Suga, *Polaronic Behavior of Photoelectron Spectra of Fe_3O_4 Revealed by Both Hard X-ray and Extremely Low Energy Photons*, J. Phys. Soc. Jpn. **79**, 064710 (2010).
41. P.A.A. van der Heijden, P.J.H. Bloemen, J.M. Gaines, J.T.W.M. van Eemeren, R.M. Wolf, p.j. van der Zaag, and W.J.M. de Jonge, *Magnetic interface anisotropy of MBE-grown ultra-thin (001) Fe_3O_4 layers*, J. Magn. Magn. Mater. **159**, L293 (1996).
 42. Y. Zhou, Ciaran McEvoy, R. Ramos, and I. V. Shvets, *The magnetic and magnetoresistance properties of ultrathin magnetite films grown on MgO substrate*, J. Appl. Phys. **99**, 608J111 (2006).
 43. G. F. M. Gomes, T. E. P. Bueno, D. E. Parreiras, G. J. P. Abreu, A. de Siervo, J. C. Cezar, H.-D. Pfannes, and R. Paniago, *Magnetic moment of Fe_3O_4 films with thicknesses near the unit cell size*, Phys. Rev. B **90**, 134422 (2014).
 44. M.A. James, F.C. Voogt, L. Niesen, O.C. Rogojanu, and T. Hibma, *The role of interfacial structure in determining magnetic behaviour in MBE-grown Fe_3O_4 /MgO multilayers on MgO(001)*, Surf. Sci. **402-404**, 332 (1998).
 45. F. C. Voogt, T. T. M. Palstra, L. Niesen, O. C. Rogojanu, M. A. James, and T. Hibma, *Superparamagnetic behavior of structural domains in epitaxial ultrathin magnetite films*, Phys. Rev. B **57**, R8107 (1998).
 46. S. K. Arora, Han-Chun Wu, R. J. Choudhary, I. V. Shvets, O. N. Mryasov, Hongzhi Yao, and W. Y. Ching, *Giant magnetic moment in epitaxial Fe_3O_4 thin films on MgO(100)*, Phys. Rev. B **77**, 134443 (2008).
 47. S. S. P. Parkin, T. Venkatesan, private communication.
 48. Yu. S. Dedkov, U. Rüdiger, and G. Güntherodt, *Evidence for the half-metallic ferromagnetic state of Fe_3O_4 by spin-resolved photoelectron spectroscopy*, Phys. Rev. B **65**, 064417 (2002).

Figures:

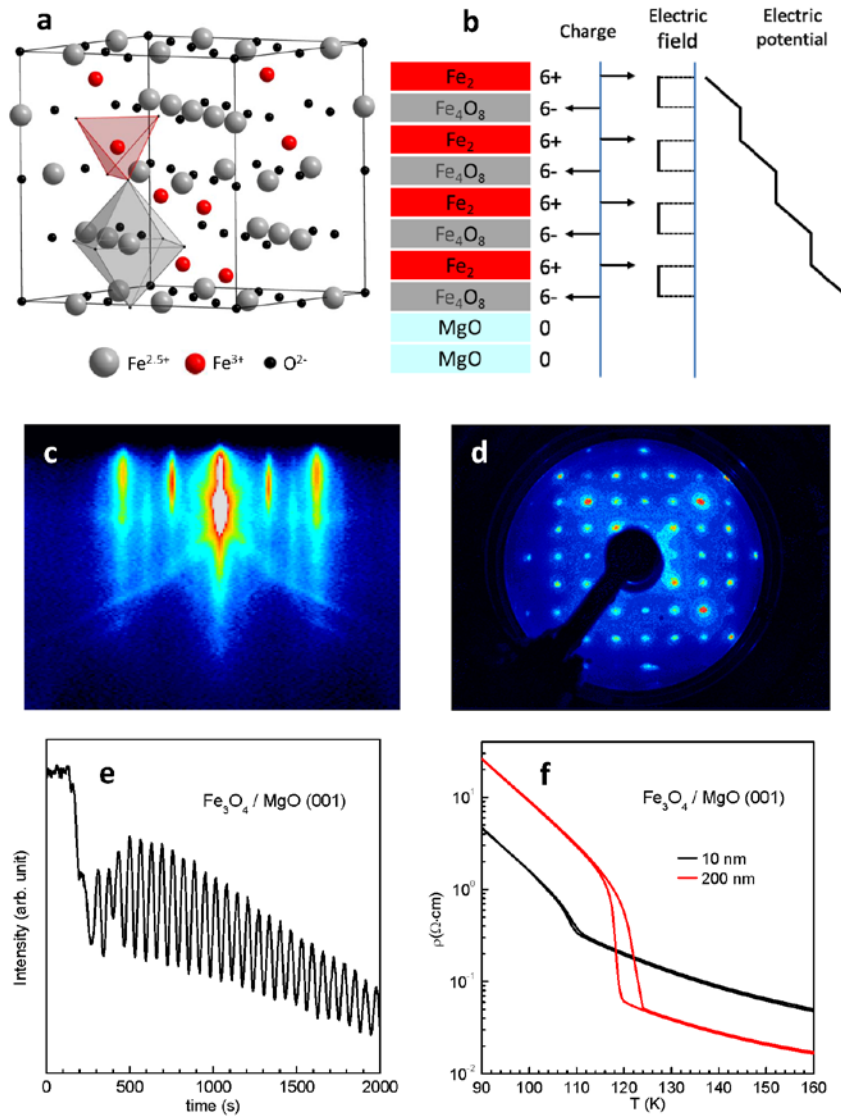


Fig. 1. Fe₃O₄ on MgO (001). (a) structure of Fe₃O₄. (b) build-up of the polar catastrophe of Fe₃O₄ on MgO (001): charged planes, and corresponding charge, electric field, and electric potential. (c) and (d) RHEED and LEED patterns, respectively, of a 200 nm epitaxial Fe₃O₄ (001) film showing the characteristic $(\sqrt{2} \times \sqrt{2})R45^\circ$ superstructure. (e) RHEED intensity oscillations of the specularly reflected beam. The electron beam was incident along the [100] direction, with a primary energy of 20 kV. (f) resistivity as a function of temperature of a 10 nm and a 200 nm thin film, showing the presence of the Verwey transition.

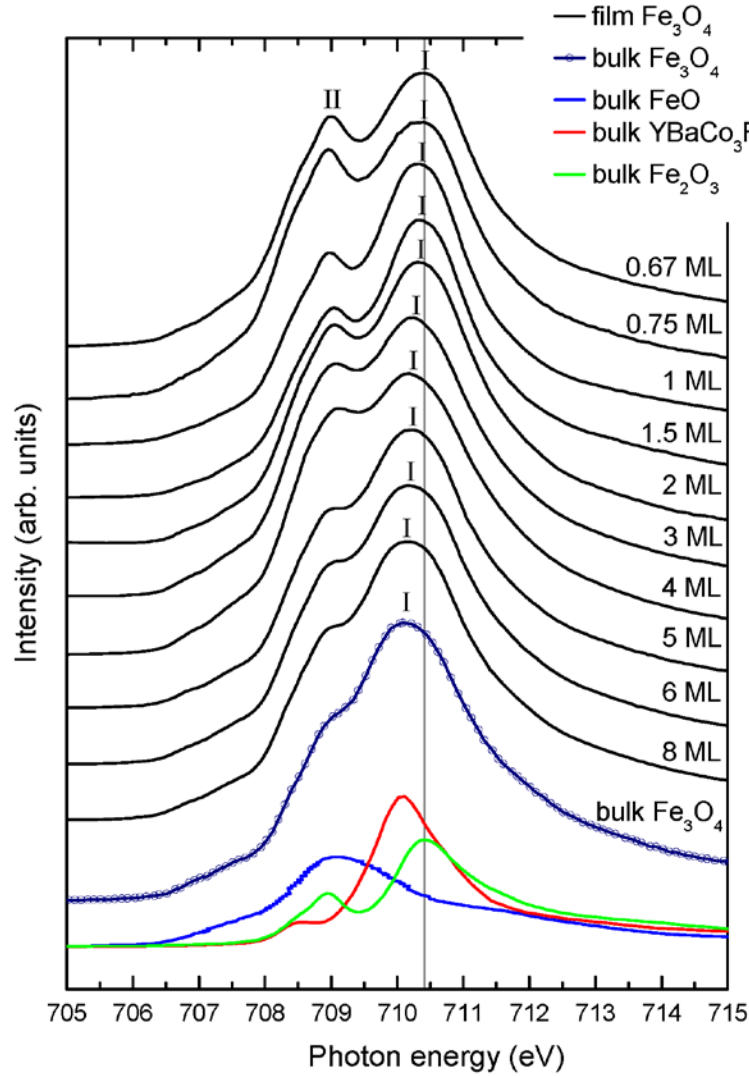


Fig. 2. Fe L_3 XAS spectra of Fe_3O_4 films. The film thickness varies from 0.67 to 8 ML. The reference spectra of bulk Fe_3O_4 , bulk $\text{YBaCo}_3\text{FeO}_7$ (Fe^{3+} in tetrahedral coordination) [28], bulk FeO (Fe^{2+} in octahedral coordination) [32] and bulk Fe_2O_3 (Fe^{3+} in octahedral coordination) are also included. All spectra were measured at 300 K. The gray line indicates the energy position of the main peak in the spectrum of bulk Fe_2O_3 . The full Fe $L_{2,3}$ spectral range is presented in the Supplementary Materials.

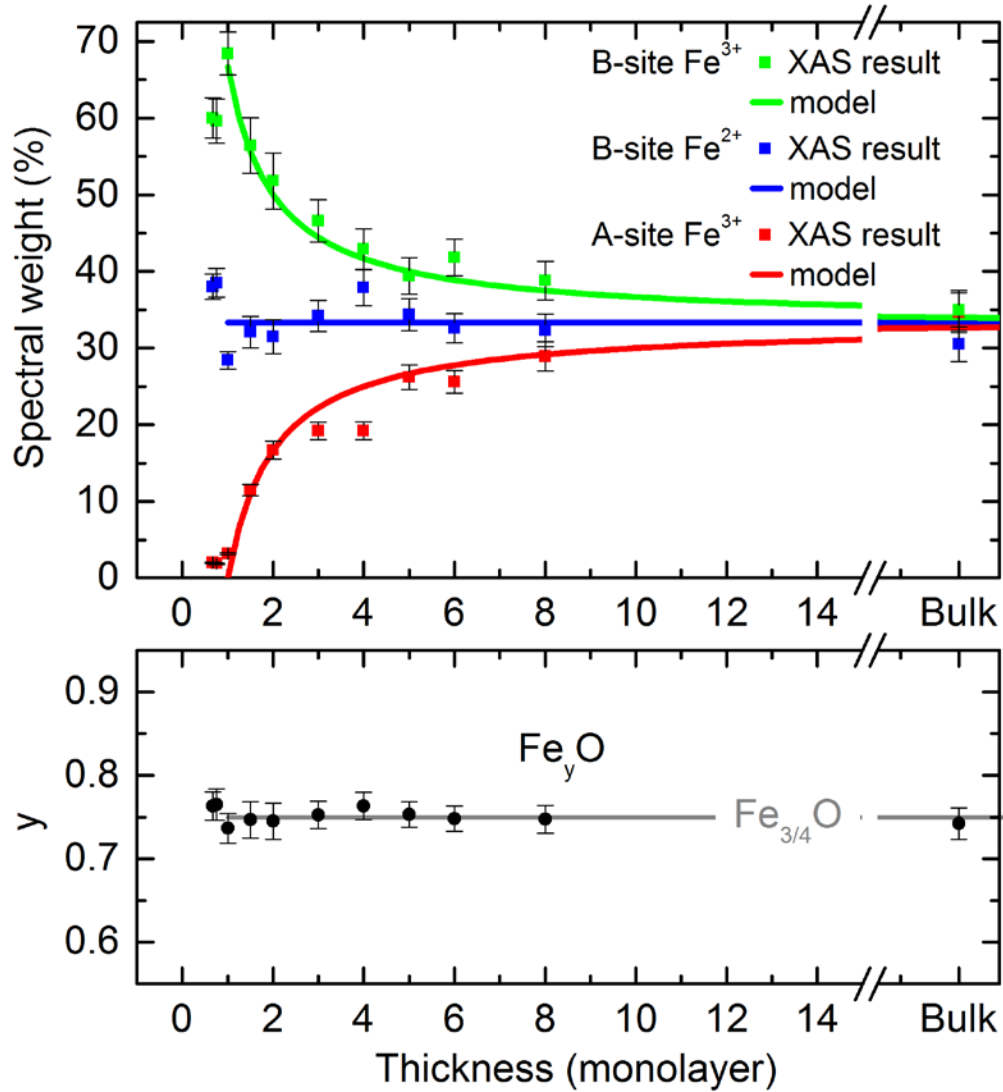


Fig. 3. The extracted spectral weight of each Fe site versus the film thickness. The spectral weight of the B-site Fe^{3+} , the B-site Fe^{2+} , and the A-site Fe^{3+} are given by the green, blue, and red closed squares, respectively. Green, blue, and red curves depict the concentrations of the B-site Fe^{3+} , the B-site Fe^{2+} , and the A-site Fe^{3+} , respectively, in our model, see the text. The Fe content (y) of the Fe_yO films derived from the average valence are shown in the bottom panel. The error bars reflect the deviations of the fits to the experimental data.

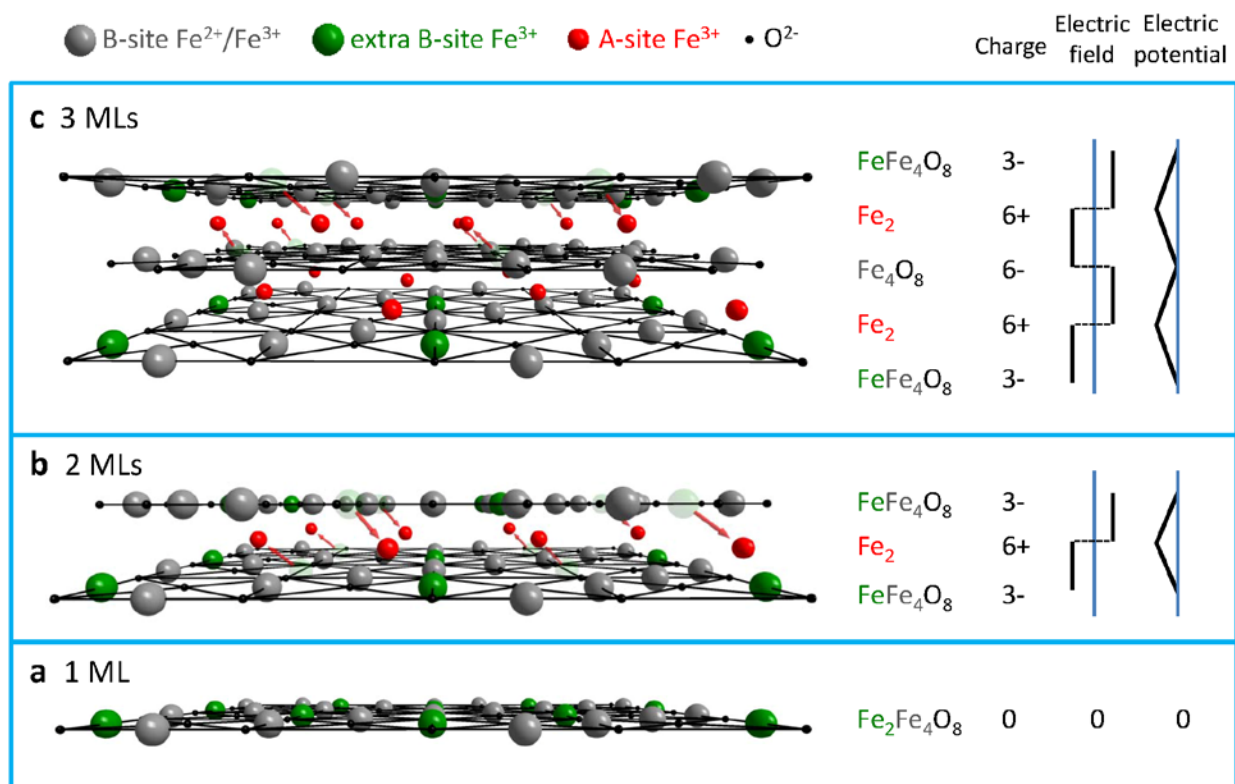


Fig. 4. Model for the growth process of polar Fe_3O_4 (001) thin films. (a) 1 monolayer, (b) 2 monolayers, and (c) 3 monolayers.

Supplementary materials:

Dynamic atomic reconstruction: how Fe₃O₄ thin films evade polar catastrophe for epitaxy

C. F. Chang,¹ Z. Hu,¹ S. Klein,^{2,†} X. H. Liu,¹ R. Sutarto,^{2,†} A. Tanaka,³ J. C. Cezar,^{4,†}
N. B. Brookes,⁴ H.-J. Lin,⁵ H. H. Hsieh,⁶ C. T. Chen,⁵ A. D. Rata,^{1,†} and L. H. Tjeng¹

Thin film growth and XAS measurement. Fe₃O₄ thin films were epitaxially grown by molecular beam epitaxy (MBE). The base pressure of the MBE system was in the low 10⁻¹⁰ mbar range. High purity Fe metal was evaporated from an alumina crucible in a pure oxygen atmosphere of 3×10⁻⁷ mbar onto clean and annealed MgO (001) substrates. The substrate temperature was kept at 250 °C during growth. *In-situ* and *real-time* monitoring of the epitaxial growth was performed by reflection high energy electron diffraction (RHEED). Oscillations in the RHEED specular beam intensity, where each oscillation corresponds to the formation of one new atomic monolayer (ML), allows for precise control of the film thickness. The RHEED oscillation measurements were done using cleaved MgO substrates, all other thin film results in this paper were obtained from epi-polished MgO substrates. The XAS measurements were performed at the 11 A Dragon beamline of the National Synchrotron Radiation Research Center (NSRRC) in Taiwan using *in-situ* MBE grown samples. The spectra were recorded at 300 K using the total electron yield method (TEY) in a chamber with a base pressure of 2×10⁻¹⁰ mbar. The photon energy resolution at the Fe *L*_{2,3} edges ($h\nu \sim 700\text{--}740$ eV) was set at 0.3 eV and the degree of linear polarization was 99%. The samples were mounted on a holder which was tilted with respect to the incoming beam, such that the Poynting vector of the light makes an angle of 70° with respect to the [001] surface normal. The angle (θ) between the electric field vector E and the [001] surface normal can be varied between 20° and 90°. I_{\parallel} and I_{\perp} are the spectra measured at $\theta = 20^\circ$ and 90° , respectively. The isotropic XAS spectra can be obtained via the formula of $I = I_{\parallel} + 2I_{\perp}$, where I_{\parallel} is the spectrum with the E parallel to the [001] surface normal extracted from $I_{\parallel} = [I_{\text{ip}} - I_{\perp}\cos^2(70^\circ)]/\sin^2(70^\circ)$. Magnetic circular dichroism (MCD) spectra of bulk magnetite crystals were measured at the ID8 beamline of the European Synchrotron Radiation Facility (ESRF) in Grenoble. The magnetic field was set at 5 Tesla. Fig. S1 shows the full Fe *L*_{2,3} XAS spectra of the Fe₃O₄ films together with the spectra of bulk Fe₃O₄, bulk YBaCo₃FeO₇ (Fe³⁺ in

tetrahedral coordination) [1], bulk FeO (Fe^{2+} in octahedral coordination) [2] and bulk Fe_2O_3 (Fe^{3+} in octahedral coordination): the spectra are identical to those in Figure 2 in the main text, but with a wider photon energy window covering both Fe L_3 and L_2 edges.

Configuration interaction cluster calculation. To interpret and better understand the x-ray absorption (XAS) spectra and their thickness dependence we have performed simulations using the well established configuration interaction cluster model that includes the full atomic multiplet theory and the local effects of the solid [3-5]. It accounts for the intra-atomic Fe $3d-3d$ and $2p-3d$ Coulomb and exchange interactions, the atomic $2p$ and $3d$ spin-orbit couplings, the O $2p$ -Fe $3d$ hybridization and the local ionic crystal field. The calculations were done using the program XTLS 8.3 [5]. The XAS spectra of Fe_3O_4 can be decomposed into the three sub-spectra of the three Fe sites, *i.e.* A-site Fe^{3+} , B-site Fe^{2+} , and B-site Fe^{3+} . We have considered an FeO_4 and an FeO_6 cluster for each Fe A-site and B-site, respectively. Parameters for the multipole part of the Coulomb interactions were given by 75% and 80% of the Hartree-Fock values for the $d-d$ and $p-d$ Slater integrals, respectively, while the monopole parts (U_{dd} , U_{cd}) as well as the O $2p$ -Fe $3d$ charge transfer energy (Δ) were adopted from typical values for Fe^{2+} and Fe^{3+} ions [6,7]. The hopping integrals between the Fe $3d$ and O $2p$ were calculated for the various Fe-O bond lengths according to Harrison's description [8]. The Fe-O bond lengths were taken from x-ray single-crystal structure diffraction data [9]. The crystal field parameter $10Dq$ was tuned to fit the experimental spectra. All parameters are listed in Ref. 10.

Figure S2 shows the experimental Fe $L_{2,3}$ XAS (open circle) and magnetic circular dichroism (MCD, open diamond) spectrum of bulk Fe_3O_4 together with the simulation results (magenta and purple lines, respectively). The three components, the sum of circular polarization spectra of each site, *i.e.* B-site Fe^{2+} (blue line), A-site Fe^{3+} (red line), and B-site Fe^{3+} (green line) are also depicted. The relative energy positions for the three sub-spectra were determined in such a way that the simulated total MCD spectrum fits by the experimental MCD spectrum best, see Refs. 6, 11, and 12. The fits were done using the "NMimimize" function of the Mathematica software [13].

By making weighted sums with the three isotropic sub-spectra using the "NMimimize" function

of the Mathematica software [13] to obtain the best fit to the experimental spectrum of each Fe film with the different thicknesses, we extract the relative amount of B-site Fe^{2+} , A-site Fe^{3+} , and B-site Fe^{3+} ions as a function of film thickness. The XAS simulation results of the Fe_3O_4 thin films of 0.67, 0.75, 1, 1.5, 2, 3, 4, 5, 6, and 8 MLs are shown in Fig. S3.

To double check the validity of the three isotropic sub-spectra, we compare them in Figure S4 with the experimental XAS spectra of the standard references for each Fe site, i.e., bulk $\text{YBaCo}_3\text{FeO}_7$ [1] for the A-site Fe^{3+} , bulk FeO [2] for the B-site Fe^{2+} , and bulk Fe_2O_3 for the B-site Fe^{3+} (same as those shown in Figure 2 in the main text, and in Figure S1 in the supplementary materials). Each of them reproduces the experimental spectrum of its corresponding reference very well. We include also in Figure S4 the XAS spectrum from $\text{Fe}_{0.04}\text{Mg}_{0.96}\text{O}$ [14], a system of Fe impurities embedded in MgO. The identical spectral features of the bulk FeO and of the Fe impurity system clearly demonstrate that XAS is most sensitive to the presence of the nearest neighbor ligands only. We have also done calculations for an Fe^{2+} in FeO_5 and an Fe^{3+} in FeO_5 by simply removing the apical oxygen of the FeO_6 , but otherwise using the same parameters as those for FeO_6 , as shown in Figure S4. Only minor differences can be observed between the isotropic XAS spectra of an Fe^{2+} in FeO_6 and in FeO_5 , and of an Fe^{3+} in FeO_6 and FeO_5 . The large difference between the isotropic XAS spectra of octahedral Fe^{3+} and tetrahedral Fe^{3+} originates from the fact that the effective $10Dq$ ligand/crystal field value is positive for the octahedral coordination while it is negative for the tetrahedral coordination.

1 ML Fe_3O_4 thin film: polarization dependence. Figure S5 shows the experimental linear polarization-dependent Fe $L_{2,3}$ XAS spectra of the 1 ML Fe_3O_4 . In the bottom panel, the experimental linear dichroic (LD) signal, defined as the difference between two polarizations ($E \parallel C - E \perp C$) is displayed, together with the calculated LD spectrum for the scenario of 33 % B-site Fe^{2+} and 67 % B-site Fe^{3+} . The LD signal can be well reproduced without including any contribution from the A-site Fe^{3+} ion. All this can be very well understood: the isotropic spectrum is determined mostly by the octahedral part of the ligand/crystal field, while the dichroism is due to the small tetragonal part of the crystal field in the monolayer. This tetragonal part of the crystal field makes the orbital occupation of the high-spin d^6 ion to become anisotropic, resulting in the polarization dependence of the intensity of the Fe^{2+} signal. The tetragonal part of the crystal field

does not affect the orbital occupation of the spherical high-spin d^5 ion but sets up the energy splitting in the XAS final states, resulting in the polarization dependence of the Fe^{3+} peak position. Please note that these XAS spectra and the dichroism therein are very different from those of Fe atoms on MgO [15], confirming the notion that $L_{2,3}$ -XAS is indeed an extremely powerful method to determine the local electronic structure of transition metal systems.

1 ML Fe_3O_4 thin film capped with 10 ML MgO. Fig. S6 shows the Fe $L_{2,3}$ -XAS spectra of the 1 ML Fe_3O_4 film, the 1 ML Fe_3O_4 film capped with 10 ML MgO, and the $\text{Fe}_{0.04}\text{Mg}_{0.96}\text{O}$ system [14]. One can clearly observe that the spectrum of the 1 ML Fe_3O_4 changes drastically upon capping with MgO and that the spectrum becomes identical to that of octahedral Fe^{2+} in $\text{Fe}_{0.04}\text{Mg}_{0.96}\text{O}$. This means that the presence of Mg converts all available Fe^{3+} into Fe^{2+} , indicating that the 1 ML $\text{Fe}^{2+}\text{Fe}^{3+}\text{Fe}^{3+}\text{O}_4$ film is reacted to 1 ML $\text{Mg}^{2+}\text{Fe}^{2+}\text{Fe}^{2+}\text{Fe}^{2+}\text{O}_4$. This in turn establishes that the 1 ML Fe_3O_4 film is indeed an $\text{Fe}_{0.75}\text{O}$ monolayer, i.e. an FeO monolayer with 25% Fe vacancies

$(\sqrt{2} \times \sqrt{2})\text{R}45^\circ$ surface reconstruction. The Fe_5O_8 surface as proposed from our model is consistent with the $(\sqrt{2} \times \sqrt{2})\text{R}45^\circ$ superstructure of the surface as shown in Fig. S7. Starting with the nonpolar Fe_6O_8 monolayer, all Fe ions are in an octahedral coordination. It consists of a bulk Fe_4O_8 layer and two extra octahedral Fe cations. Every other extra octahedral Fe cation is then removed to help to form the A-site layer below. The remaining extra octahedral Fe ions in the Fe_5O_8 surface layer can then be arranged as to give the $(\sqrt{2} \times \sqrt{2})\text{R}45^\circ$ superstructure. In Fig. S7 we also have included the directions (arrows) of the atomic relaxations forming a wavelike surface patterns along the $[110]$.

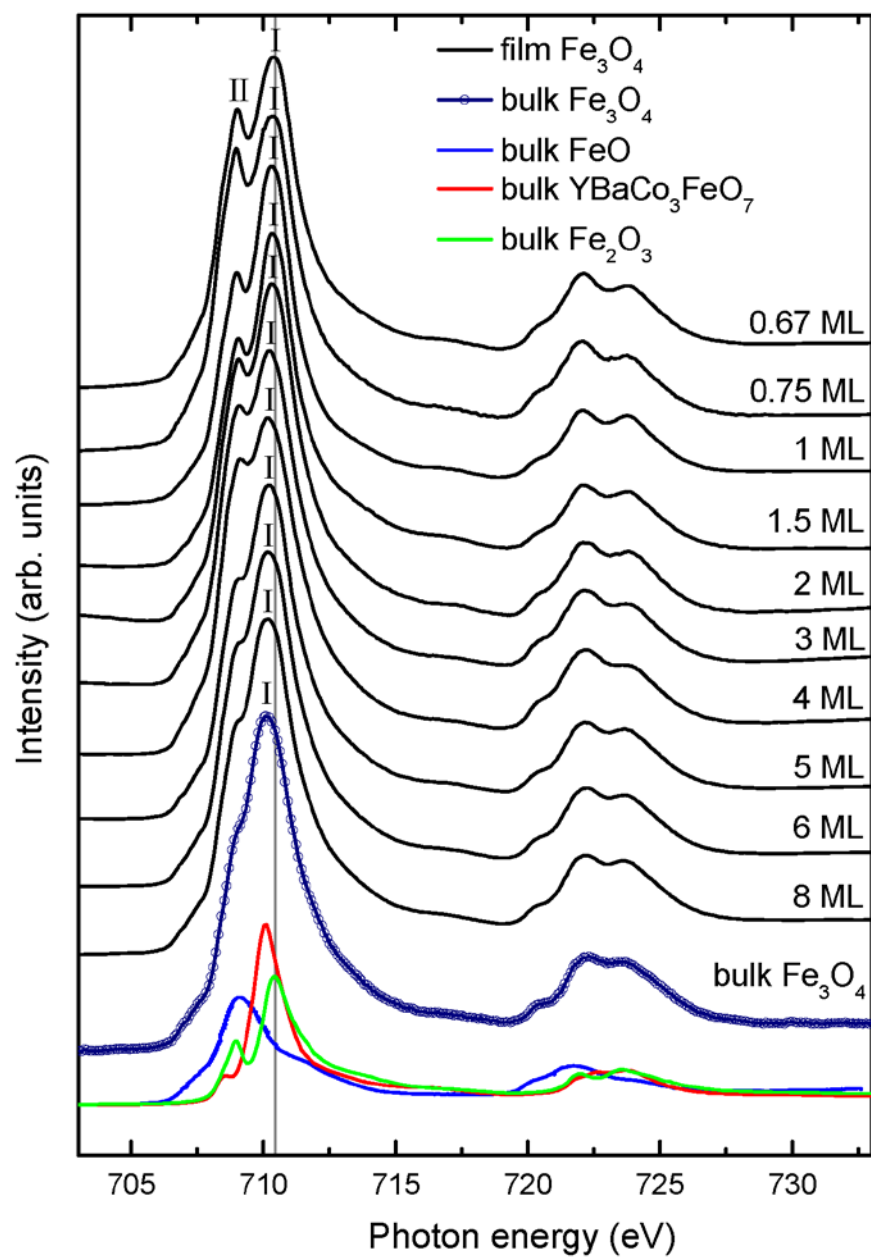


Figure S1. The full range of the Fe $L_{2,3}$ XAS spectra depicted in Fig. 2.

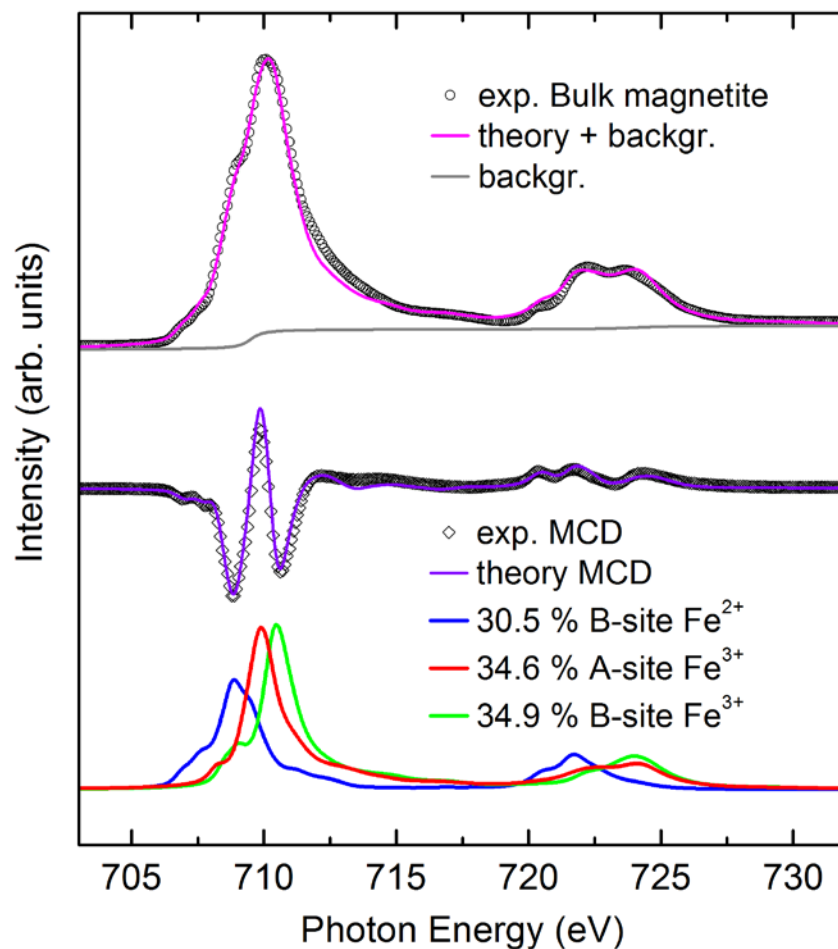
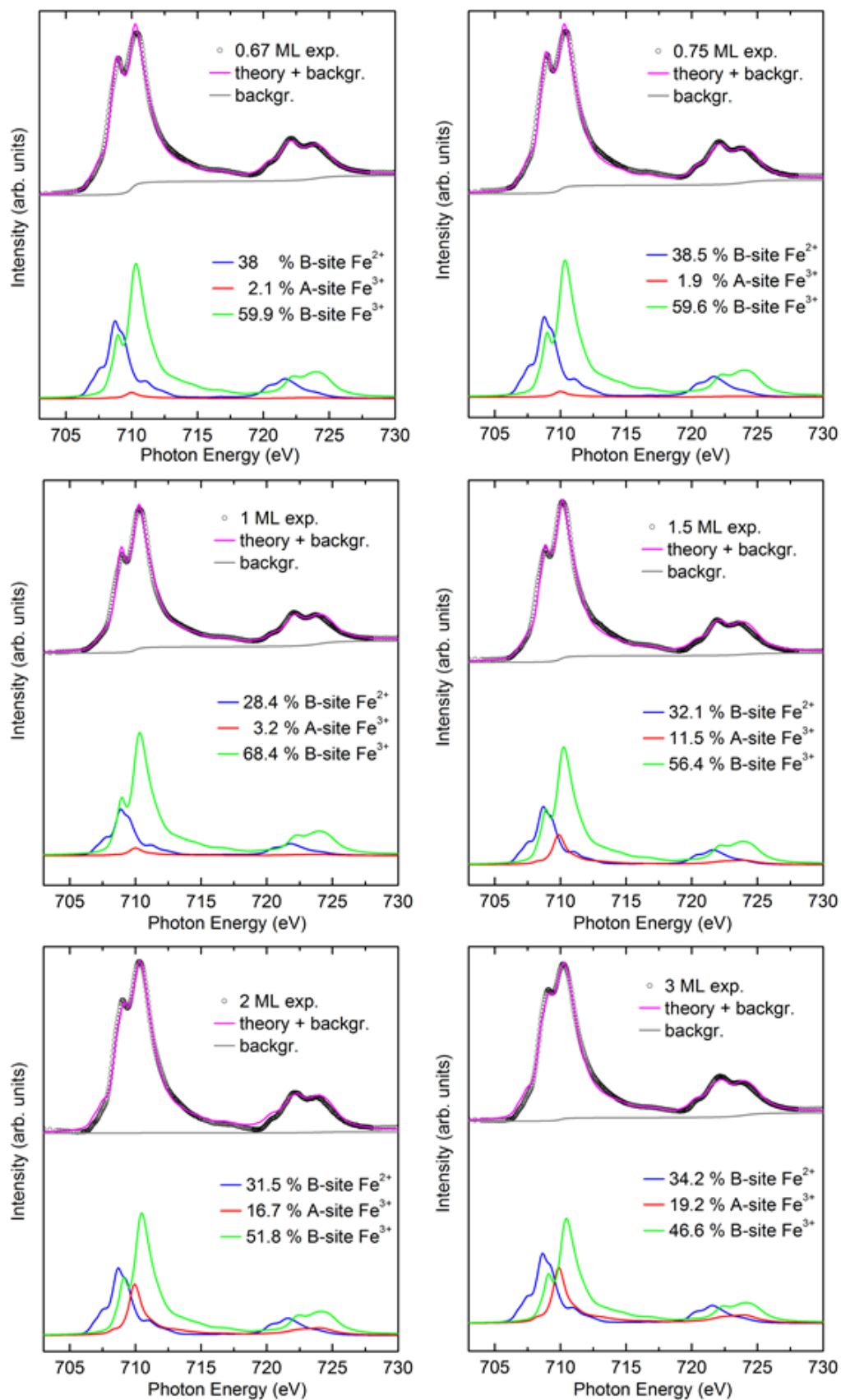


Figure S2. Fe $L_{2,3}$ XAS and MCD spectra of bulk Fe_3O_4 . The XAS (open circle) and MCD spectra (open diamond) were taken at 300 K. Magenta and purple curves are the simulated XAS and MCD spectra, respectively. The gray line is an arctangent like XAS background. Simulations for the three components are displayed in the bottom panel: B-site Fe^{2+} (blue line), A-site Fe^{3+} (red line), and B-site Fe^{3+} (green line).



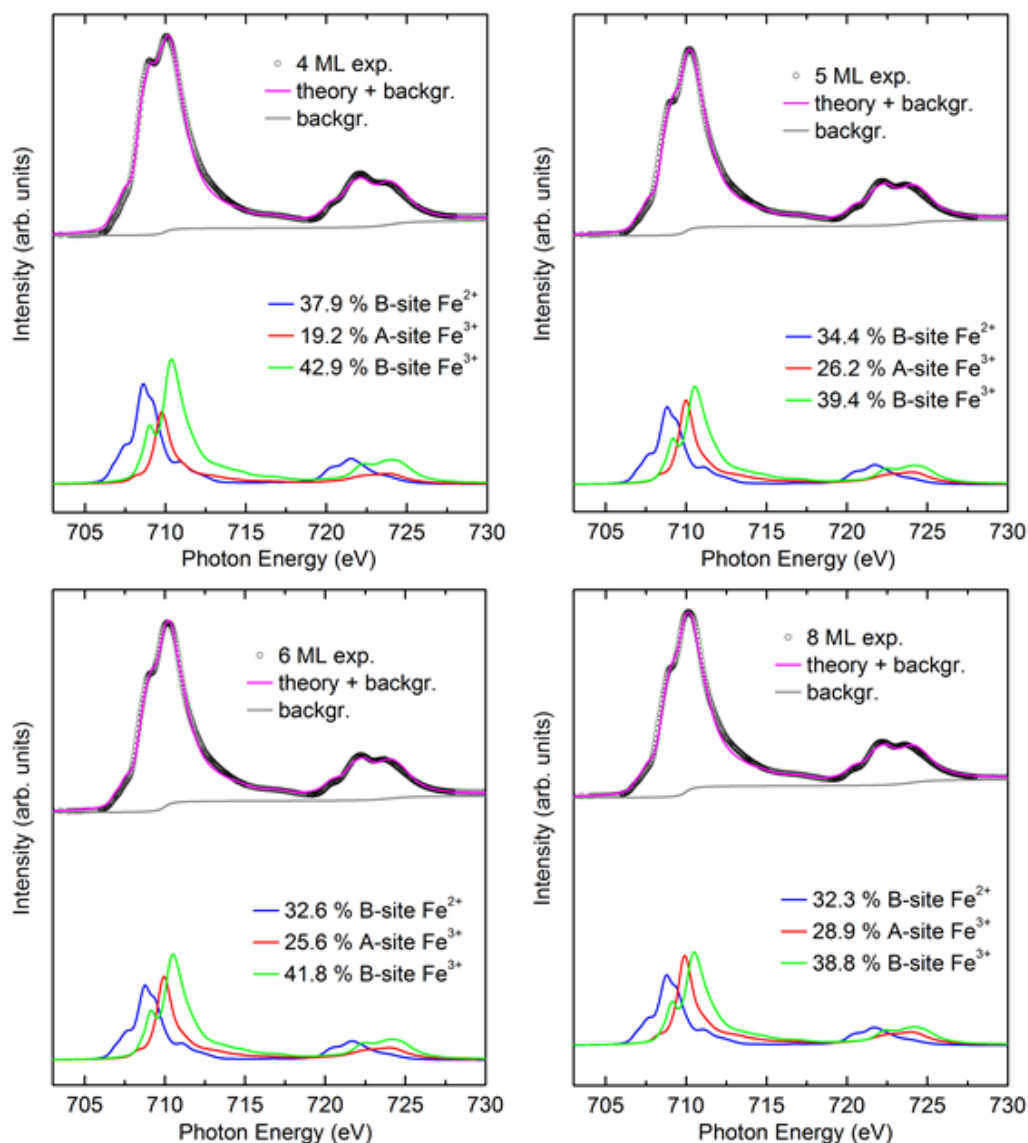


Figure S3. The XAS simulation results of the Fe_3O_4 thin films of 0.67, 0.75, 1, 1.5, 2, 3, 4, 5, 6, and 8 MLs. The experimental XAS (open circle) spectra are those in Fig. S1. The magenta curve is the simulated XAS spectrum. The gray line is an arctangent like XAS background. Simulations for the three components are displayed in the bottom panel: B-site Fe^{2+} (blue line), A-site Fe^{3+} (red line), and B-site Fe^{3+} (green line).

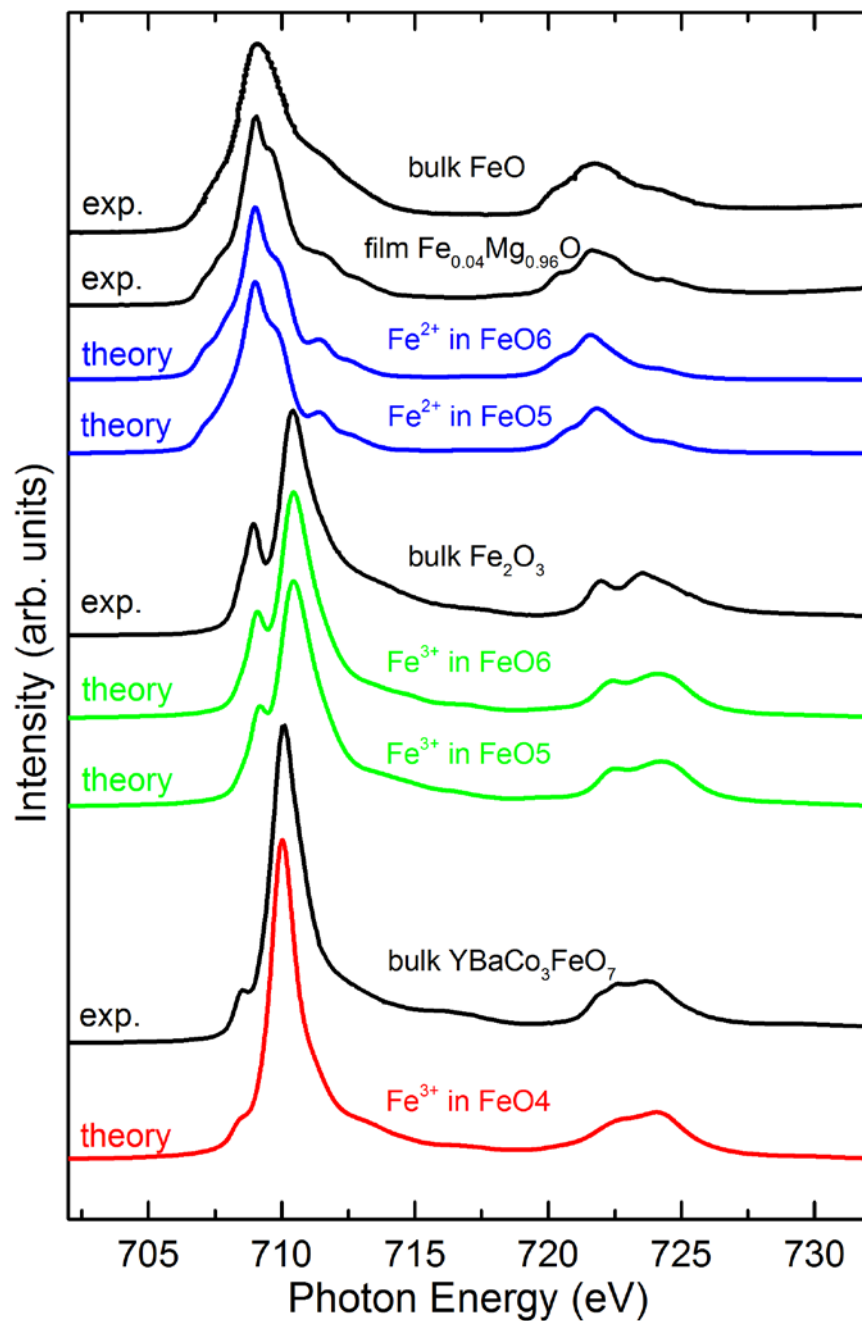


Figure S4. Experimental Fe $L_{2,3}$ XAS spectra of bulk FeO [2] (Fe^{2+} in octahedral coordination), thin film $\text{Fe}_{0.04}\text{Mg}_{0.96}\text{O}$ [13] (Fe^{2+} in octahedral FeO6), bulk Fe_2O_3 (Fe^{3+} in octahedral FeO6), and bulk $\text{YBaCo}_3\text{FeO}_7$ [1] (Fe^{3+} in tetrahedral FeO4), together with the simulated spectra of an Fe^{2+} in FeO6 and in FeO5, an Fe^{3+} in FeO6 and FeO5, and an Fe^{3+} in FeO4.

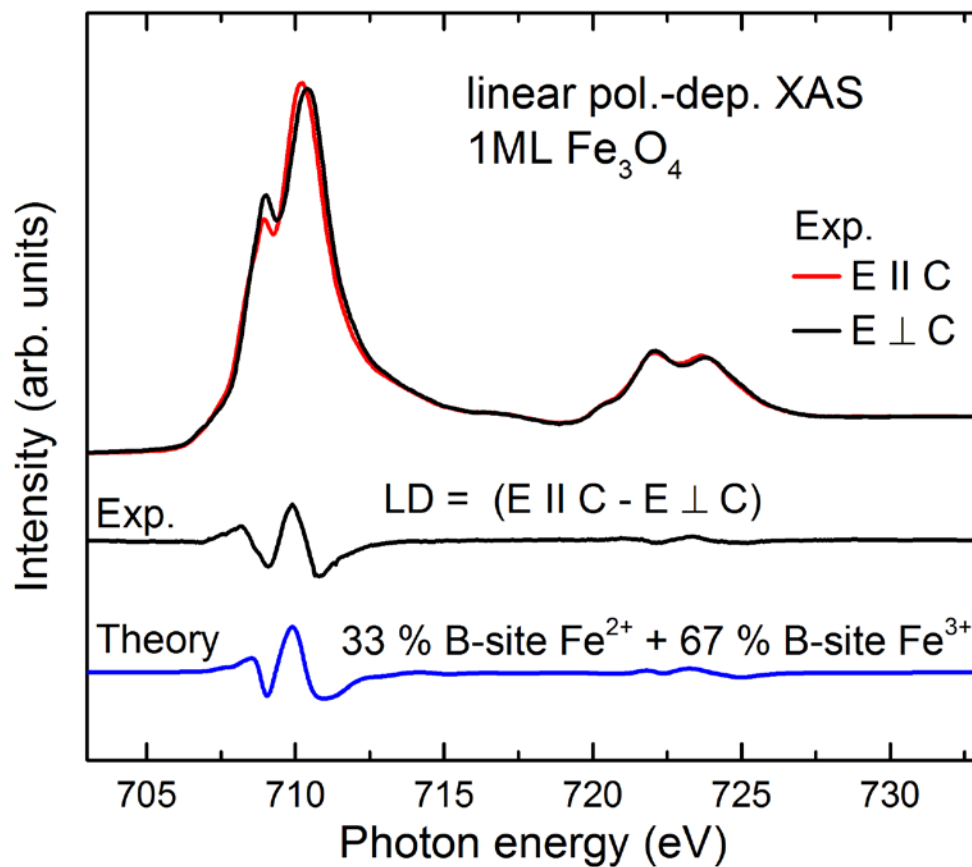


Figure S5. Experimental linear polarization-dependent Fe $L_{2,3}$ XAS spectra of 1 ML Fe_3O_4 . The experimental linear dichroic (LD) signal defined as the difference between two polarizations ($E \parallel C - E \perp C$) is shown in the middle, together with the calculated LD spectrum for the scenario of 33 % B-site Fe^{2+} and 67 % B-site Fe^{3+} (no A-site Fe^{3+}).

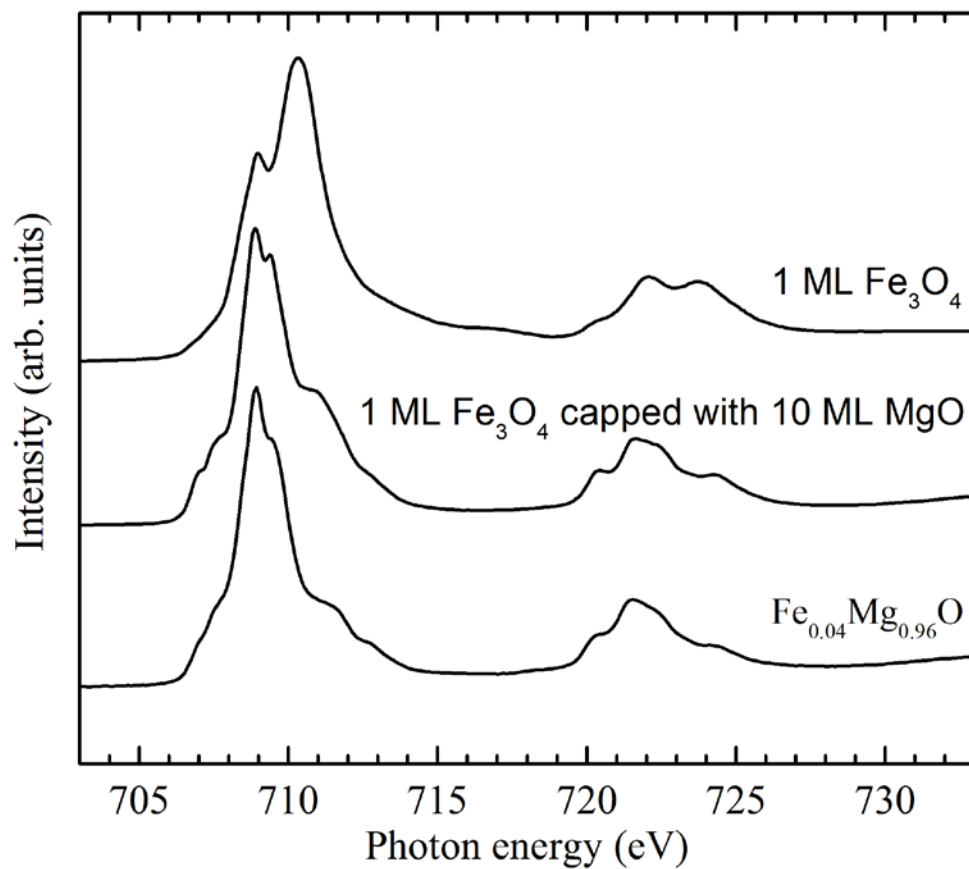


Figure S6. Fe $L_{2,3}$ XAS spectra of the 1 ML Fe_3O_4 , the 1 ML Fe_3O_4 capped with 10 ML MgO, and $\text{Fe}_{0.04}\text{Mg}_{0.96}\text{O}$ thin film.

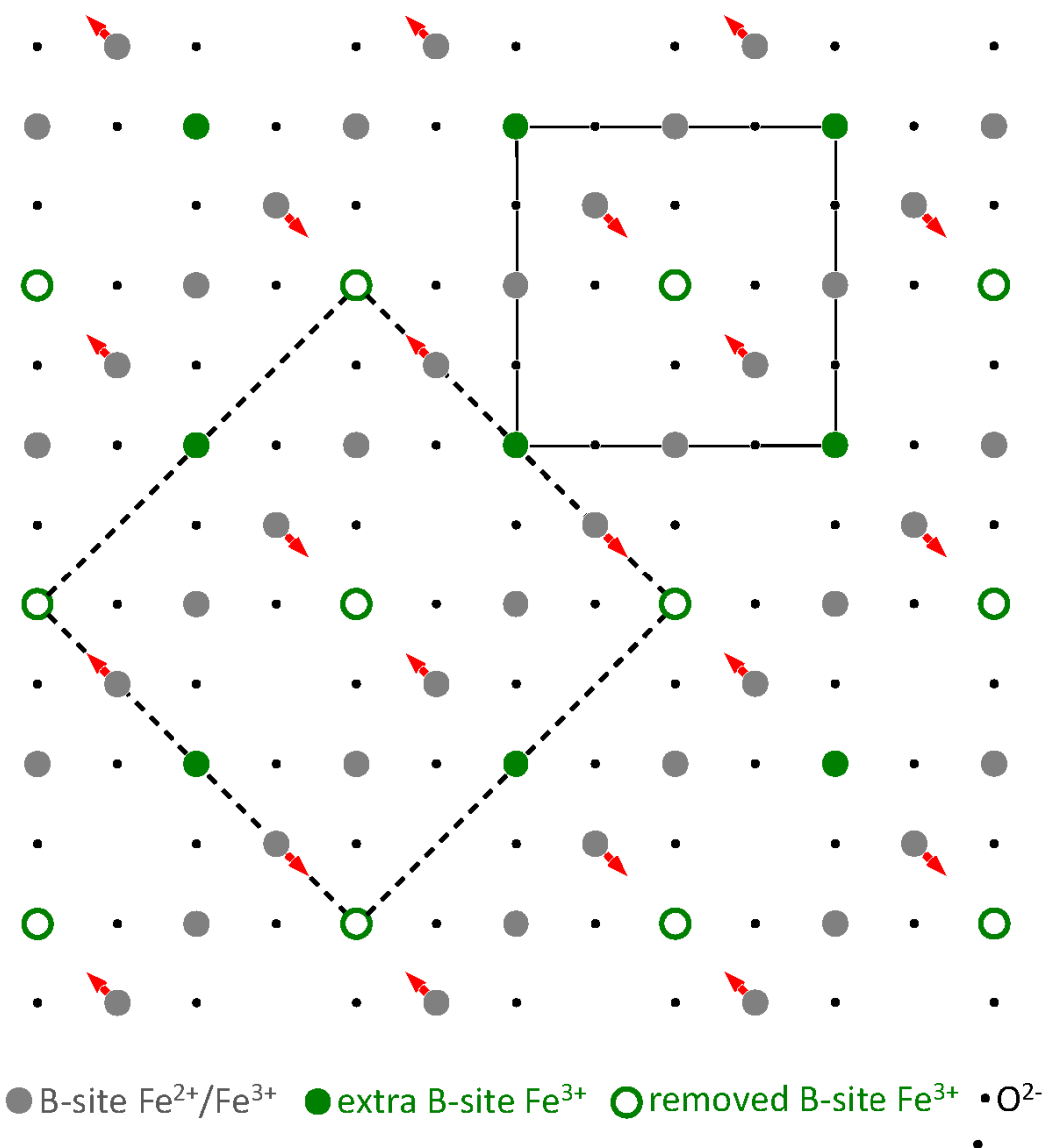


Figure S7. Proposed $(\sqrt{2} \times \sqrt{2})\text{R}45^\circ$ surface reconstruction of Fe_3O_4 (001). The solid-line square is the conventional cubic unit cell. The dashed-line square is the superstructure unit cell. Also included are the directions (arrows) of the atomic relaxations forming a wavelike surface patterns along the $[110]$.

References of the Supplementary materials

1. N. Hollmann, Z. Hu, M. Valldor, A. Maignan, A. Tanaka, H. H. Hsieh, H.-J. Lin, C. T. Chen, and L. H. Tjeng, Electronic and magnetic properties of the kagome systems YBaCo_4O_7 and $\text{YBaCo}_3\text{MO}_7$ ($\text{M}=\text{Al}, \text{Fe}$), Phys. Rev. B **80**, 085111 (2009).
2. J. H. Park, Ph.D. thesis, University of Michigan (1994).
3. F. M. F. de Groot, X-ray absorption and dichroism of transition metals and their compounds, J. Electron Spectrosc. Relate. Phenom. **67**, 529 (1994).
4. Theo Thole Memorial Issue, J. Electron Spectrosc. Relate. Phenom. **86**, 1 (1997).
5. A. Tanaka and T. Jo, Resonant 3d, 3p and 3s Photoemission in Transition Metal Oxides Predicted at 2p Threshold, J. Phys. Soc. Jpn. **63**, 2788 (1994).
6. J. Chen, D. J. Huang, A. Tanaka, C. F. Chang, S. C. Chung, W. B. Wu, and C. T. Chen, Magnetic circular dichroism in Fe 2p resonant photoemission of magnetite, Phys. Rev. B **69**, 085107 (2004).
7. A. E. Bocquet, T. Mizokawa, K. Morikawa, A. Fujimori, S. R. Barman, K. Maiti, and D. D. Sarma, Y. Tokura, and M. Onoda, Electronic structure of early 3d-transition-metal oxides by analysis of the 2p core-level photoemission spectra, Phys. Rev. B **53**, 1161 (1996).
8. W. A. Harrison, *Electronic Structure and the Properties of Solids* (Dover, New York, 1989).
9. Jon P. Wright, J. Paul Attfield, and Paolo G. Radaelli Charge ordered structure of magnetite Fe_3O_4 below the Verwey transition, Phys. Rev. B **66**, 214422 (2002).
10. Parameters for A-site Fe^{3+} FeO_4 cluster [eV]: $U_{dd}= 6.0$, $U_{cd}= 7.5$, $\Delta= 3.5$, $10Dq= -0.2$; parameters for B-site Fe^{2+} FeO_6 cluster [eV]: $U_{dd}= 6.0$, $U_{cd}= 7.5$, $\Delta= 7.0$, $10Dq= 0.6$; parameters for B-site Fe^{3+} FeO_6 cluster [eV]: $U_{dd}= 6.0$, $U_{cd}= 7.5$, $\Delta= 3.0$, $10Dq= 0.6$. $10Dq$ is the ionic part of the crystal field splitting which is defined as the energy difference between the x^2-y^2 and the xy orbitals. An exchange field of 70 meV was applied to account for the ferrimagnetic order; positive for the B-sites and negative for the A-site.
11. P. Kuiper, B.G. Searle, L.-C. Duda, R.M. Wolf, and P.J. van der Zaag, Fe $L_{2,3}$ linear and circular magnetic dichroism of Fe_3O_4 , J. Electron Spectrosc. Relate. Phenom. **86**, 107 (1997).

12. Alessandro Mirone, Maurizio Sacchi, and Susana Gota, Ligand-field atomic-multiplet calculations for arbitrary symmetry, *Phys. Rev. B* **61**, 13540 (2000).
13. Wolfram Research, Inc., Mathematica, Version 8.0, Champaign, IL (2010).
14. T. Haupricht, R. Sutarto, M. W. Haverkort, H. Ott, A. Tanaka, H. H. Hsieh, H.-J. Lin, C. T. Chen, Z. Hu, and L. H. Tjeng, Local electronic structure of Fe^{2+} impurities in MgO thin films: Temperature-dependent soft x-ray absorption spectroscopy study, *Phys. Rev. B* **82**, 035120 (2010).
15. S. Baumann, F. Donati, S. Stepanow, S. Rusponi, W. Paul, S. Gangopadhyay, I. G. Rau, G. E. Pacchioni, L. Gragnaniello, M. Pivetta, J. Dreiser, C. Piamonteze, C. P. Lutz, R. M. Macfarlane, B. A. Jones, P. Gambardella, A. J. Heinrich, and H. Brune, Origin of Perpendicular Magnetic Anisotropy and Large Orbital Moment in Fe Atoms on MgO, *Phys. Rev. Lett.* **115**, 237202 (2015).